Reac Kinet Mech Cat (2017) 122:117–133
DOI 10.1007/s11144-017-1196-9

The chemoselective hydrogenation of crotonaldehyde over PtFe catalysts supported on $La_2O_2CO_3$ nanorods

Fengjun Hou[1,2] · Huanling Song[1] · Huahua Zhao[1] · Jun Zhao[1] · Jian Yang[1] · Liang Yan[1] · Lingjun Chou[1,3]

Received: 20 February 2017 / Accepted: 13 May 2017 / Published online: 29 May 2017

Abstract The PtFe catalysts supported on the $La_2O_2CO_3$ nanorods with various Fe loadings are constructed at the atomic level. The composition and structure of the resultant catalysts are analyzed by ICP-OES, XRD, TEM, H_2-TPR, H_2-TPD and XPS techniques. A subsequent study of crotonaldehyde hydrogenation over the catalysts shows that the iron addition exerts great influence on the catalyst structure and the associated reactive performance. The surface oxygenated groups of $La_2O_2CO_3$ afford a high dispersion of Pt due to the interfacial confinement effect. The Pt-support interfaces are wrecked by Fe atoms located on the catalyst surface, simultaneously producing bimetallic surfaces. Both surface studies and catalytic reaction experiment on the catalysts illustrate that an increased electronic density on Pt and the structure evolution of metal particles upon Fe addition is tentatively proposed to be accounted for the distinct catalytic behaviors. Under the working conditions, the highest selectivity toward the desired crotyl alcohol of the Fe-promoted catalysts is two-fold higher than that of the Pt/$La_2O_2CO_3$.

Keywords $La_2O_2CO_3$ nanorods · Platinum-iron · Bimetallic structure · Crotonaldehyde hydrogenation

Electronic supplementary material The online version of this article (doi:10.1007/s11144-017-1196-9) contains supplementary material, which is available to authorized users.

✉ Lingjun Chou
ljchou@licp.cas.cn

[1] State Key Laboratory for Oxo Synthesis and Selective Oxidation, Lanzhou Institute of Chemical Physics, Chinese Academy of Sciences, Lanzhou 730000, People's Republic of China

[2] University of Chinese Academy of Sciences, Beijing 100049, People's Republic of China

[3] Suzhou Research Institute of LICP, Chinese Academy of Sciences, Suzhou 215123, People's Republic of China

Introduction

The chemoselective hydrogenation of α,β-unsaturated aldehydes to unsaturated alcohols is an important step for the production of pharmaceutical and fine chemicals [1, 2]. However, this selective hydrogenation process is challenging since the activation and hydrogenation of C=O bond is unfavorable over its conjugated C=C bond in the viewpoint of thermodynamic aspects [3]. Therefore, achieving a high yield of unsaturated alcohol by designing a novel catalyst with high efficiency and durability is highly desired. As one of the most intensively studied system developed, Pt catalysts perform good activity but poor selectivity toward the unsaturated alcohol. The selectivity enhancement toward the production of the unsaturated alcohol usually can be achieved by using an active support [4–11], modulating the size and morphology of active metal [5, 12], or adding a more electropositive metal [13–15].

It is known that the chemical composition and structure of a support greatly affects the catalytic performance of its supported catalyst by influencing the size, morphology and electronic states of active metal/interfacial species. The utilization of an active support is considered to favor the formation of strong metal-support interaction (SMSI), thus changing the adsorption and hydrogenation of crotonaldehyde (CRAL) molecules. Vannice et al. reported that Pt–TiO_x interfacial sites of Pt/TiO_2 favored the polarization and hydrogenation of the C=O bond [4]. On the other hand, the Pt (111) epitaxial layer on CeO_2, instead of Pt–CeO_x interfacial sites or CePt sites, was suggested to be the catalytic sites for the hydrogenation of C=O bond [5]. Lercher's group concluded that either large Pt particles with high fraction of Pt (111) surfaces or TiO_x decorated Pt sites was responsible for the enhanced selectivity toward unsaturated alcohol [16]. Kennedy et al. compared the sum-frequency generation vibrational spectroscopy for Pt/TiO_2 and Pt/SiO_2, and proposed that a crotyl-oxy surface intermediate through the aldehyde oxygen atom binding to an oxygen vancancy (O_{vac}) site on the TiO_2 surface, should be responsible for the additional catalytic activity and C=O selectivity of Pt/TiO_2 relative to Pt/SiO_2 [17].

Besides, doping Pt with a more electropositive metal is proposed to effectively improve the catalytic activity, selectivity or stability. Generally, incorporating a second metal M into a Pt catalyst can modify the electronic and geometric properties of Pt owing to a ligand effect or an ensemble size effect [18–20]. The first effect is based on the observation of an increased electron density on Pt due to the electron transfer from M to Pt. The increased electron density on Pt is claimed to decrease the probability of C=C bond adsorption, and at the same time, to increase the interaction of the C=O bond with the polar bimetallic sites [18, 21, 22]. For the second one, the unreduced MO_x species situated at the edge and corner sites of Pt particles acts as Lewis acid adsorption sites for the aldehyde groups [14, 15, 20, 23]. The ensemble size effect is also observed with proper geometric type of the bimetallic surfaces by a complex set of factors [18, 24, 25]. Various Pt-based bimetallic catalysts have been developed and found to display prominent performance for α,β-unsaturated aldehyde hydrogenation. However, due to the

sensitivity of bimetallic nanostructures to the support materials and synthetic parameters, there is no consistent picture for active sites in the bimetallic catalysts.

Lanthanum oxy-carbonate ($La_2O_2CO_3$) has drawn much attention for its impressive activity in the oxidative coupling of methane, steam reforming of glycerol and biofuel production [26–29]. As previously reported by our group, the preferential deposit of Pt on the {110} facets of $La_2O_2CO_3$ nanorods (LOC-NR) displayed superior catalytic behavior for CRAL hydrogenation to that on the particle-counterpart [30]. However, Pt/LOC is limited by the low selectivity (22.8%) to the desired crotyl alcohol (CROL). Herein, a series of PtFe/LOC catalysts with various Fe amount are developed to improve the hydrogenation selectivity of carbonyl groups in the CRAL molecules. Noticeably, an enhanced selectivity toward CROL is attained over the resultant PtFe/LOC catalysts compared to that on the Pt/LOC. The combined experimental and analytical investigations show that Fe addition induces the electronic and geometric changes of surface metals, which are accounted to be responsible for the preferential adsorption and hydrogenation of C=O bonds. Correlating detailed characterizations with the catalytic reaction study, we gain new information about the structure–activity relationship of the bimetallic PtFe/LOC catalysts.

Experimental

Catalyst preparation

LOC-NR was obtained by the thermal transformation of lanthanum hydroxide nanorods at 500 °C for 3 h [30]. The specific surface area of LOC-NR was 45 $m^2\ g^{-1}$, as calculated on the basis of the Barrett-Joiner-Halenda (BJH) method. Monometallic Pt/LOC and Fe/LOC were synthesized via an incipient wet impregnation process through the impregnation of LOC-NR with metal precursors ($H_2PtCl_6{\cdot}6H_2O$ and $Fe(NO_3)_3{\cdot}9H_2O$). After aging and drying at 120 °C for 10 h, the obtained powders were calcined at 400 °C for 2 h, followed by reduction at 600 °C for 1 h under a flowing gas mixture of 20% H_2/N_2 (v/v). The Fe/Pt/LOC series catalysts with nominal Fe loadings of 0.25, 0.40, 0.50, and 0.75 wt % were prepared through the impregnation of the dried Pt/LOC with $Fe(NO_3)_3$ ethanol solution following an identical procedure, and denoted as *x*Fe/Pt/LOC ($x = 0.25$, 0.40, 0.50, or 0.75).

Catalyst characterization

The actual loadings of metals were analyzed on inductively coupled plasma optical emission spectrometry (ICP-OES) on an Agilent 725-ES.

The phase identification of the catalysts was recorded on an X'Pert Pro Multipurpose diffractometer (PANalytical, Inc.) using Ni-filtered Cu K_α radiation (0.15406 nm) with a scanning angle (2θ) range of 10–80°, conducted at 40 kV and 20 mA.

Morphological analysis of the catalysts was conducted on the TECNAI G2 F20 high-resolution transmission electron microscopy operated at 200 kV. The size distributions of metal particles over the catalysts were assessed from the observation of more than 300 particles in TEM images. The mean diameter was calculated by the following formula: $d_s = \sum nidi^3 / \sum nidi^2$.

XPS spectra were acquired using a Thermo Scientific ESCALAB250xi spectrometer to determine the chemical states and surface atomic composition of the catalysts. All binding energies were referenced to C 1*s* hydrocarbon peak at 284.8 eV. The surface atomic concentration of each element was calculated from the area of the corresponding peak. The deconvolution of Pt 4*f* spectra was processed with a curve-fitting routine using the XPSPEAK41 software. The integral of each peak was determined after the subtraction of the background and fitting with some constrains on the fitting parameters including the half width height maximum (FWHM = 1.43), peak area ratio (Pt $4f_{7/2}$: Pt $4f_{5/2}$ = 4:3) and position (the binding energy gap between Pt $4f_{7/2}$ and Pt $4f_{5/2}$ peak is 3.35 eV) with a combination of Gaussian (80%) and Lorentzian (20%) functions.

Experiments on the temperature-programmed reduction (TPR) and desorption (TPD) of hydrogen were taken on a ChemBET Pulsar TPR/TPD analyzer (Quantachrome Instruments U.S.) equipped with a TCD detector. Typically, 50 mg unreduced sample was loaded in a U-tube quartz reactor and pretreated at 400 °C for 30 min in flowing Ar (40 mL min^{-1}); after cooling the reactor to 40 °C, the TPR experiment was carried out from room temperature to 900 °C with a ramp of 20 °C min^{-1} in flowing 7% H_2/Ar (40 mL min^{-1}). The TPD curves of the reduced catatlysts (50 mg) was obtained from room temperature to 900 °C at a ramp of 20 °C min^{-1} in flowing Ar (40 mL min^{-1}) after hydrogen-adsorption at 70 °C for 60 min.

Catalytic performance evaluation

Catalytic reaction was carried out in a stainless high pressure reactor of 100 mL capacity, in which 1 mL of CRAL was hydrogenated using 150 mg of catalyst and 24 mL of ethanol. After purging four times with hydrogen, the catalytic test was conducted at 70 °C with a hydrogen pressure of 2.0 MPa. The products were analyzed using an Agilent GC-7890A equipped with an FID detector and a HP-5 capillary column. The CRAL conversion (*Conv.*) and products selectivity (*Sel.*) were calculated as follows.

$$Conv.\mathrm{C_4H_6O} = \frac{{}^{n}\mathrm{C_4H_6O}_{(a)} - {}^{n}\mathrm{C_4H_6O}_{(b)}}{{}^{n}\mathrm{C_4H_6O}_{(a)}} \times 100\% \quad (1)$$

$$Sel._x = \frac{n_x}{{}^{n}\mathrm{C_4H_6O}_{(a)} - {}^{n}\mathrm{C_4H_6O}_{(b)}} \times 100\% \quad (2)$$

Here ${}^{n}\mathrm{C_4H_6O}_{(a)}$ and ${}^{n}\mathrm{C_4H_6O}_{(b)}$ is the amount of substance of the initial and residual CRAL, respectively. n_x is the mole of the product.

The cycle experiment was carried out under the same conditions except with the recovered catalyst. The spent catalyst was recovered from the mixture of hydrogenation system by centrifugation, desiccation at 120 °C and calcination at 300 °C for 1 h.

Results and discussion

Catalyst characterization

As revealed by the ICP-OES data in Table 1, the Pt loading of the Pt-containing catalysts is in the range of 1.25–1.32%; the Fe loading of Fe/Pt/LOC and *x*Fe/Pt/LOC catalysts is 0.48, 0.21, 0.39, 0.44, and 0.78%, which are basically consistent with the nominal values.

As shown in Fig. 1, the diffraction patterns of all catalysts can be mainly assigned to a mixture of hexagonal $La_2O_2CO_3$ (JCPDS No. 25-0424) and hexagonal La_2O_3 (JCPDS No. 02-0688). Noticeably, Pt/LOC performs a higher phase composition of La_2O_3 as indicated by the higher intensity ratio of $I_{(2\theta = 29.2^\circ)}$ to $I_{(2\theta = 26.1^\circ)}$. It is known that $La_2O_2CO_3$ holds in an arrangement of $(La_2O_2)^{n+}$ layers separated by CO_3^{2-} ions, and incorporation of a noble metal onto the lanthanum support can induce the phase transformation depending on the gas atmosphere during the thermal treatment [31–33]. Presumably, Pt adatoms onto the catalyst surface promote the phase transformation of $La_2O_2CO_3$ into La_2O_3, suggesting a strong metal-support interaction of Pt/LOC. The Fe addition inhibits this process to some extent, as indicated by the decreased diffraction signals of La_2O_3 in the Fe-promoted catalysts. No reflections associated with metals and their oxides or PtFe alloys can be detected for the supported catalysts, implying a high dispersion of metals on the catalyst surface [34, 35].

As shown in Fig. 2 and Fig. S1, the rod-like morphology of the support with diameters of 15–20 nm and lengths of 200–400 nm is well maintained for all catalysts. In the case of the Pt/LOC (in Fig. S1a and Fig. S2), Pt particles centered at 1.5 nm with a narrow size distribution in the range of 0.8–2.6 nm are uniformly dispersed on the support surface. It can be clearly observed from Fig. S1b that ellipsoidal or spheroidal particles with diameters of about 10–20 nm are distributed on the Fe/LOC catalyst surface, suggesting a weak interaction between iron oxides and the support. The HRTEM investigation identifies the lattice fringe spacing of 3.40 Å, which can be assignable to the facets of orthorhombic Fe_3O_4. TEM images

Table 1 The metal loadings of the catalysts determined by ICP-OES analysis

Catalyst	Pt (wt%)	Fe (wt%)	$n_{(Pt/Fe)}$
Fe/LOC	–	0.48	–
Pt/LOC	1.29	–	–
0.25Fe/Pt/LOC	1.32	0.21	1.80
0.40Fe/Pt/LOC	1.31	0.39	0.96
0.50Fe/Pt/LOC	1.29	0.44	0.84
0.75Fe/Pt/LOC	1.25	0.81	0.44

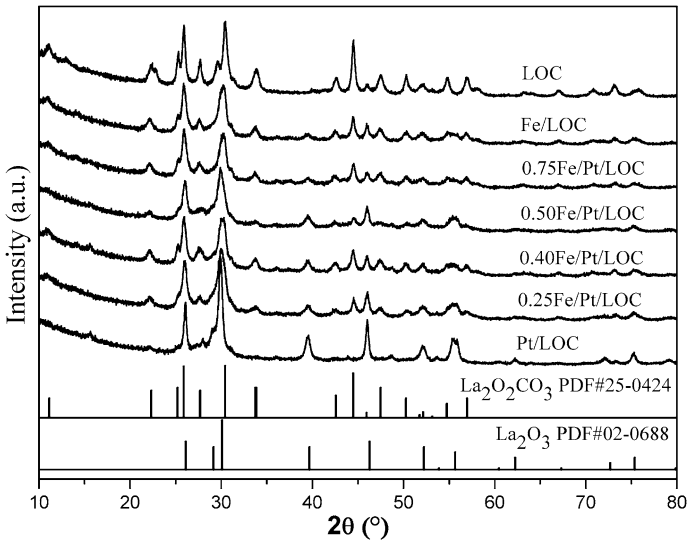

Fig. 1 Standard diffraction patterns of hexagonal $La_2O_2CO_3$ and hexagonal La_2O_3, and XRD patterns of the samples

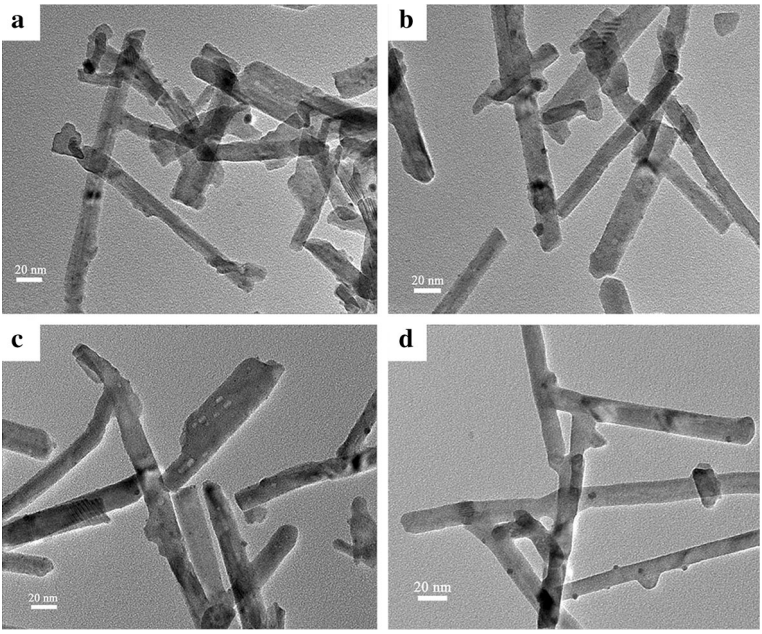

Fig. 2 TEM images of 0.25Fe/Pt/LOC (**a**), 0.40Fe/Pt/LOC (**b**), 0.50Fe/Pt/LOC (**c**) and 0.75Fe/Pt/LOC (**d**)

in Figs. 2a–2d and the statistical results in Fig. S2 demonstrate that incorporating Fe into Pt/LOC does not practically affect the size distribution of Pt particles over the *x*Fe/Pt/LOC catalysts. Noticeably, morphological analysis confirms the successful

loading of Fe on Pt/LOC and the generation of new particles related to FeO_x or Pt–FeO_x entities, whose size is determined as about 5–20 nm for 0.25Fe/Pt/LOC. As Fe loading increases, more particles with decreased size (2–10 nm for 0.75Fe/Pt/LOC) are observed. Combined with the XRD results, it can be speculated that the Fe addition may induce the migration of Pt atoms from catalyst surface to interact with iron and fracture large FeO_x particles into small ones upon H_2 reduction [36, 37].

To investigate the interaction of the surface composites over the catalyst, H_2-TPR measurement was conducted. As displayed in Fig. 3, Pt/LOC presents two reduction peaks: the first one, in the temperature range of 400–600 °C, is associated with the reductive decomposition of platinum oxychlorine and the reduction of the support surface in the vicinity of Pt centers; the second one above 700 °C can be related to the reductive decomposition of the lanthanum support [38]. It can be seen that higher temperature for Pt-containing catalysts than that of the bare LOC and Fe/LOC is needed for the reductive decomposition of the lanthanum support, suggesting a higher phase composition of La_2O_3 for the Pt-doped catalysts, which is in consistence with the XRD results. In addition, incorporating iron into the Pt/LOC decreases the peak area in the temperature region of 400–600 °C, suggesting that the bonding strength of the Pt-lanthanum interfaces is much weakened upon Fe addition. A new peak centered at 311 °C is observed at a small amount of Fe (0.25%), while two peaks centered at 305 and 280 °C appear when Fe loading increases to 0.40%. Further increasing the Fe loading, the low-temperature reduction peak starts to grow in intensity and peak area at the expense of the middle-temperature one. The emergence of new peaks at lower temperatures can be interpreted as the reductive decomposition of platinum and iron precursors, which is much lower than that of Pt/LOC (500 °C) and Fe/LOC (408 °C). It is clearly shown

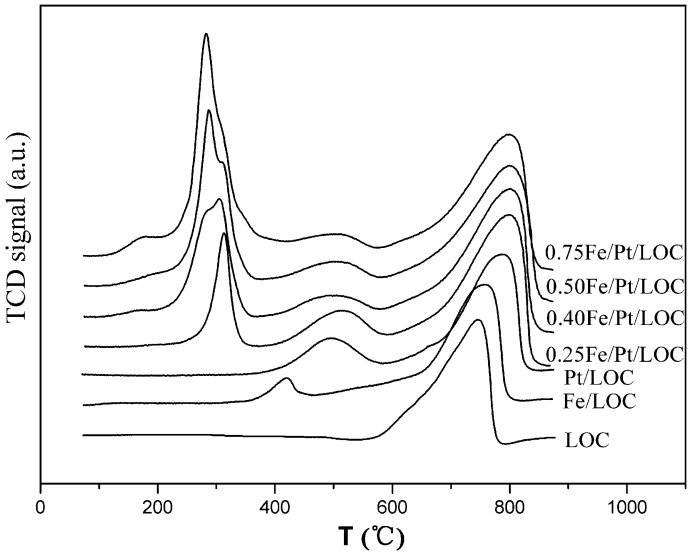

Fig. 3 H_2-TPR profiles of the samples obtained from room temperature to 900 °C with a ramp of 20 °C min^{-1} in flowing 7% H_2/Ar (40 mL min^{-1})

that the Fe addition greatly improves the reducibility of the catalysts. As TEM analyses display no difference in the size distribution of Pt particles with the Fe addition, we attribute the enhanced reducibility of the Fe-doped catalysts to the promotional effect of iron on the hydrogen spillover phenomenon. It is known that Pt can act as active adsorption sites for molecular hydrogen [5, 24]. Once dissociated, highly reactive hydrogen species (i.e. H^+, H^-, H^{3+}) spills over to reduce the support surface, and it can also be used to reduce Fe ionic species [39]. It has been documented that the reduction of a support could play an important role in the metal-support interaction, producing either reduced cations or oxygen vacancy O_{vac} sites [5, 38, 40]. The spillover of hydrogen species from platinum to the transition metal M usually induces the formation of low-coordinated MO_x species or the alloying structure [21, 39]. These two effects compete and compromise in bimetallic catalysts and influence the electronic and geometric characteristics of Pt. In conjunction with the XRD and TEM results, it is reasonable to accept that the incorporation of Fe induces the migration of Pt atoms from the Pt-lanthanum interfaces to interact with the Fe species. Then, a close contact between Pt sites and the Fe species would improve the increasing of activated hydrogen number due to the enhanced hydrogen spillover phenomenon.

Fig. 4 displays the profiles of the desorbed H_2 versus temperature for the catalysts in the temperature range of 100–900 °C. The wide desorption peaks in H_2-TPD curves appear as a result of different activation energies for desorption, indicating the surface heterogeneity of the adsorption sites. It can be seen that there is an analogous peak shape of hydrogen desorption on the $La_2O_2CO_3$ and La_2O_3, which initiates from 250 °C and the peak maximum concentrated at 400–600 °C.

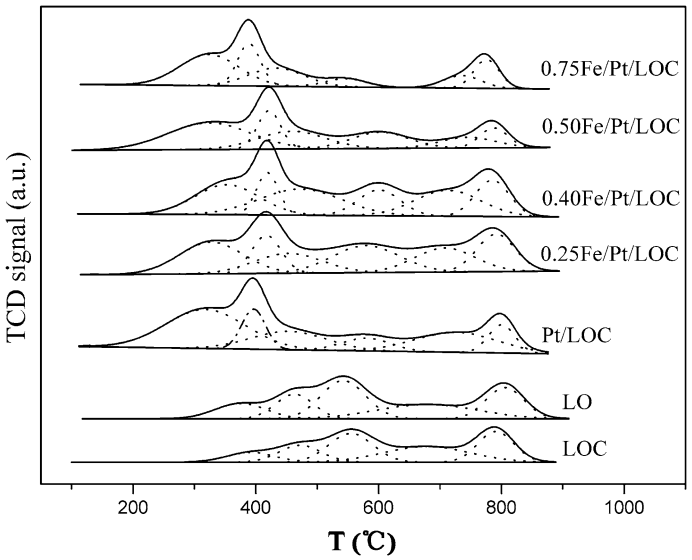

Fig. 4 H_2-TPD profiles of the samples. Each *curve-fitting* is processed after subtraction of the baseline from the TPD data and then deconvolution into *six* peaks to isolate the contributions of H_2 desorption sites from different surface structures

The desorption temperature of hydrogen on the supported metal catalysts can be divided into three regions: the low-temperature range of 200–500 °C initiates from the hydrogen desorption from metal sites, the mid-temperature one in the region of 500–700 °C stems from the hydrogen desorption from the support surface, and the high-temperature peak above 700 °C originates from the thermal decomposition of $La_2O_2CO_3$ [41]. In the case of Pt/LOC, the low-temperature peak can be deconvoluted into three peaks centered at 318, 396 and 454 °C, which can be assigned to hydrogen desorbed from the different kinds of active metal sites. Quantification of total H_2 desorption below 500 °C for Pt/LOC is 3.15 mmol g_{Pt}^{-1} (listed in Table 2). When the Fe loading increases from 0.25 to 0.75%, the amount of hydrogen desorption from metal sites decreases continuously from 2.95 to 2.42 mmol g_{Pt}^{-1}. The variation in the composition and structure of active sites usually contributes to the desorption behavior of hydrogen. It is reported that the MO_x deposits preferentially onto the low-coordinated Pt sites at small amount of iron, which in consequence reduces the exposure degree of Pt sites [42, 43]. In this sense, it is suggested that the Fe-promoted catalyst has a lower Pt accessibility than Pt/LOC because of the site blocking effect of Pt by the Fe species.

The surface chemical composition and valences of as-prepared catalysts are analyzed by XPS measurement. The fresh Pt/LOC for the Pt $4f_{7/2}$ and Pt $4f_{5/2}$ lines exhibit a distinct asymmetric shape inclined toward high binding energies and the peak area ratios deviate from the theoretical value of 1.33, suggesting the different chemical states of Pt. As shown in Fig. S3 and Table 3, the Pt $4f_{7/2}$ spectra for the Pt/LOC catalyst can be deconvoluted into two features as metallic Pt^0 (71.8 eV) and oxidized Pt^{2+} species (73.6 eV), and the Pt^{2+}/Pt^0 ratio is 0.44. The higher binding energy value of Pt^0 relative to that of pure Pt foil has been observed by decreasing the particle size of Pt clusters due to the quantum size effect [44]. The oxidized Pt^{2+} is reported to be originated from the strong coordination of Pt with the oxygen atoms of the support or the residual chlorine species on the catalyst surface [34, 45–47]. The broad and weak peak at 710.6 eV of Fe 2*p* spectra for the Fe/LOC and *x*Fe/Pt/LOC catalysts demonstrates the co-existence of Fe(II) and Fe(III) ionic species. Additionally, the Fe addition lowers the binding energy of platinum in the 0.25Fe/Pt/LOC at a shift of 0.3 eV, and at the same time the Pt^{2+}/Pt^0 ratio is decreased to 0.31. As suggested by the XRD and H_2-TPR results, some Pt–O bonds

Table 2 The H_2-TPD results of the samples

Catalyst	Amount of desorbed hydrogen (mmol g_{Pt}^{-1})			
	Peak 1	Peak 2	Peak 3	Total
LO	–	0.28	0.42	0.70
LOC	–	0.16	0.31	0.47
Pt/LOC	1.80	0.55	0.80	3.15
0.25Fe/Pt/LOC	1.33	0.74	0.88	2.95
0.40Fe/Pt/LOC	1.42	0.57	0.77	2.76
0.50Fe/Pt/LOC	1.61	0.57	0.55	2.73
0.75Fe/Pt/LOC	1.17	0.61	0.64	2.42

Table 3 The surface atomic composition and chemical states of the catalysts from XPS measurements

	Pt $4f_{7/2}$			Atomic ratio (mol/mol)			
	BE (eV)	species	%	Pt^{2+}/Pt^0	Pt/La	Pt/Fe	O/La
Fe/LOC	–	–	–		–	–	2.87
Pt/LOC	71.8	Pt^0	69.3	0.44	0.021	–	3.04
	73.6	Pt^{2+}	30.7				
0.25Fe/Pt/LOC	71.6	Pt^0	76.2	0.31	0.021	0.69	3.18
	73.3	Pt^{2+}	23.4				
0.40Fe/Pt/LOC	71.6	Pt^0	81.2	0.24	0.014	0.44	3.09
	73.6	Pt^{2+}	19.8				
0.50Fe/Pt/LOC	71.5	Pt^0	81.9	0.22	0.017	0.39	2.89
	73.5	Pt^{2+}	18.1				
0.75Fe/Pt/LOC	71.4	Pt^0	87.4	0.14	0.018	0.37	2.67
	73.2	Pt^{2+}	12.6				
Pt/LOC-C	71.7	Pt^0	78.3	0.28	0.021	–	2.62
	73.5	Pt^{2+}	21.7				
0.50Fe/Pt/LOC-C	71.8	Pt^0	62.2	0.61	0.020	0.20	2.58
	73.7	Pt^{2+}	37.8				

at the Pt–lanthanum interfaces are broken upon Fe addition, which facilitates the reduction of oxidized Pt^{2+} to metallic Pt^0. The negative shift of Pt 4*f* spectra for the iron-promoted catalysts can be attributed to the improved Pt–Fe interaction upon Fe addition, which improves the increasing of highly active hydrogen number and results into the presence of electronic-rich Pt.

The quantified elemental distributions over catalyst surface are outlined in Table 3. It is noteworthy that the Pt/Fe ratios of bimetallic catalysts analyzed by XPS are much lower than those from ICP analyses, suggesting the surface enrichment of iron. Furthermore, the decreased O/La ratios with increasing Fe composition imply that more O_{vac} sites are produced owing to the enhanced hydrogen spillover phenomenon upon iron addition [25].

Evaluation of the catalytic properties

CRAL hydrogenation is chosen as a probe reaction to evaluate the catalytic behavior of the resultant catalysts. As shown in Fig. 5, CRAL is mainly hydrogenated to butyraldehyde (BUAL, hydrogenation product of C=C bond), crotyl alcohol (CROL, hydrogenation product of C=O bond), and saturated hydrogenation product butanol (BUOL, hydrogenation product of C=C and C=O bond). It should be mentioned that Fe/LOC shows almost no catalytic activity. It is clear that Fe is not the active center in catalysis. The evolving catalytic hydrogenation results associated with the Fe loading from 0.25 to 0.75% are summarized in Table 4. In a reaction period of 60 min, the Pt/LOC catalyst exhibits 19.7% selectivity to CROL with 61.2% conversion of CRAL. Under the same

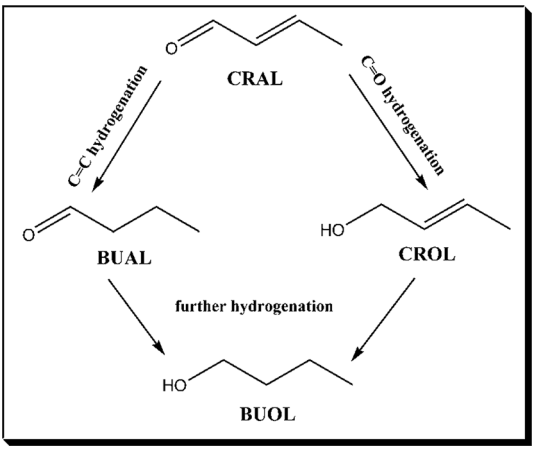

Fig. 5 Reaction pathways for CRAL hydrogenation

reaction conditions, the 0.25Fe/Pt/LOC catalyst shows the highest conversion of CRAL (99.8%), mainly from the high rates of CROL and BUOL formation. However, a further increase in Fe loadings drastically reduces the catalytic reactivity. The CRAL conversion of *x*Fe/Pt/LOC catalysts descends to 92.2, 60.8, and 36.1% when the Fe loading increases to 0.40, 0.50, and 0.75%. Impressively, the selectivity to CROL increases strongly with the promotion of iron, and reaches a maximum value (54.5%) at Fe loading of 0.75%. It should be noteworthy that the selectivity to CROL over the 0.50Fe/Pt/LOC is two-fold higher than that of the Pt/LOC in spite of their close catalytic reactivity. The explanation for this behavior may be associated with the presence of new catalytic active sites when Pt and Fe are brought into atomic contact.

The time-dependent hydrogenation results over 0.50Fe/Pt/LOC in Fig. 6 show that the desired CROL (60.1%) is the main product while the byproducts BUAL and BUOL are limited to a relatively low level when the reaction time is 20 min. As the reaction time increases, the conversion of CRAL is boosted from 31.6 to 79.8%,

Table 4 The hydrogenation results of CRAL over the catalysts

Catalyst	$Conv._{CRAL}$ (mol%)	Sel.(mol%)			$Yield_{CROL}$(%)
		BUAL	BUOL	CROL	
Fe/LOC	0.5	100.0	0.0	0.0	0.0
Pt/LOC	61.2	61.5	18.7	19.8	12.1
0.25Fe/Pt/LOC	98.8	23.4	58.0	18.8	18.6
0.40Fe/Pt/LOC	92.2	28.7	35.3	36.4	33.6
0.50Fe/Pt/LOC	60.8	30.8	16.5	52.9	32.2
0.75Fe/Pt/LOC	36.1	35.9	9.6	54.5	19.7

Reaction conditions: 150 mg of catalyst, 1 mL of CRAL, 24 mL of ethanol as solvent, $T = 70$ °C, H_2 pressure = 2.0 MPa, $t = 60$ min

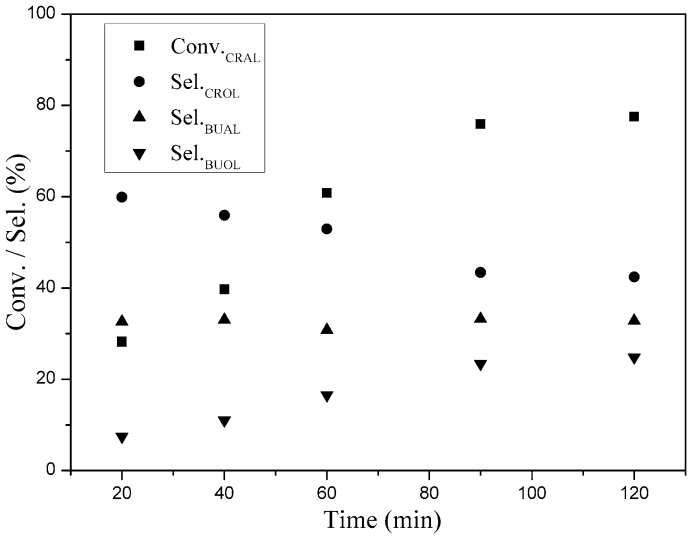

Fig. 6 Time-dependent results of CRAL hydrogenation over 0.50Fe/Pt/LOC. Reaction condition: 150 mg of catalyst, 1 mL of CRAL, 24 mL of ethanol as solvent, $T = 70$ °C, H_2 pressure = 2.0 MPa

while the selectivity to CROL decreases continuously from 60.2 to 40.1%, resulting in the further hydrogenation of CROL to BUOL.

The stability is one of the parameters to evaluate the catalytic performance of heterogeneous catalysts. The reusability of Pt/LOC and 0.50Fe/Pt/LOC is investigated, and the results are presented in Fig. 7. The Pt/LOC presents a good reproducibility, while an obvious drop in the catalytic activity and CROL selectivity of 0.50Fe/Pt/LOC is detected during the cycles. To investigate the deactivation related to the active center, the spent Pt/LOC-C and 0.50Fe/Pt/LOC-C after five cycles are collected for characterization after calcination at 300 °C for 1 h. TEM analyses of the cycled catalyst in Fig. S4 demonstrate a high dispersion of metal particles over the support surface. Pt particles on the Pt/LOC-C are confined at 1.3 nm with a narrow size distribution. By contrast, 0.50Fe/Pt/LOC-C shows the homogeneous metal particles with an average particle size of 2.1 nm, larger than the highly dispersed Pt clusters while smaller than the FeO_x or Pt–FeO_x ensembles on the fresh one. This further affirms the prevailing influence of the enhanced metal-support interaction on the stabilization of Pt particles over the Pt/LOC. As indicated by XPS in Fig. S5, the new peak at 292.2 eV in C 1*s* spectra of 0.50Fe/Pt/LOC-C clearly manifests the existence of residual organic molecules (by-products from hydrogenation reaction) on the catalyst surface, which can be readily removed from the lanthanum surfaces in the vicinity of Pt centers for Pt/LOC-C [26, 27, 48]. The carbon deposit and an increase of Pt particles is proposed to be the dominant factor for the activity drop of 0.50Fe/Pt/LOC-C [5, 24]. Platinum in the cycled catalysts composed of Pt^0 and Pt^{2+} is detected, and the Pt^{2+}/Pt^0 ratio of 0.50Fe/Pt/LOC-C is 0.61, much higher than that of the fresh one. In conjunction with the decreased Pt/Fe ratio and the uniform metal particles over the 0.50Fe/Pt/LOC-C, it is suggested the

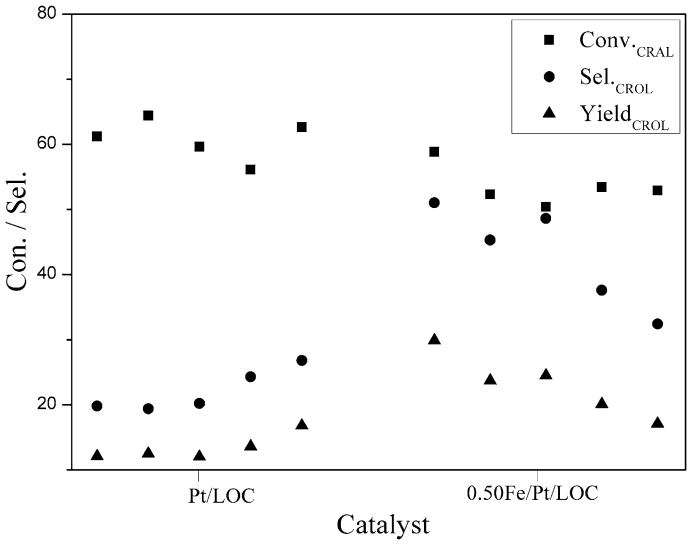

Fig. 7 Recyclability of Pt/LOC and 0.50Fe/Pt/LOC for the liquid-phase CRAL hydrogenation during *five* cycles. Reaction conditions: 150 mg of catalyst, 1 mL of CRAL, 24 mL of ethanol as solvent, $T = 70$ °C, H_2 pressure = 2.0 MPa, $t = 60$ min

structure evolution of bimetallic ensembles after five cycles of hydrogenation-oxidation treatment is accounted to be the primary reason responsible for the decreased selectivity of aldehyde hydrogenation.

Discussion

According to the reactive performance of the resultant catalysts, the Fe addition exerts great influence on the catalytic activity and selectivity of PtFe catalysts. As TEM analyses show that incorporation of Fe do not cause obvious change in the size distribution of Pt particles over the PtFe/LOC catalysts, the size effect of Pt particles is excluded from the promoting effect of Fe. Therefore, the distinct catalytic behavior of Fe-promoted catalysts most likely results from the dilution of Pt sites by FeO_x entities, which determines the adsorption mode of CRAL molecule and the hydrogenation routes.

According to the XRD, H_2-TPR and TEM results, the strong metal-support interaction is attained on the Pt/LOC. The strong metal-support interaction makes the rearrangements at the metal-support interfaces kinetically and thermodynamically limited, thus producing fine Pt particles and preventing the migration and aggregation of Pt particles. Considering the fact that the Fe/LOC and bare LOC show almost no reactivity for hydrogenation, it is reasonable to accept that platinum in the catalyst is the main active sites for adsorbing and cleaving H_2 molecule into active hydrogen species. The O_{vac} site owing to the spillover effect of Pt to lanthanum support is proposed to be the active center for the polarization of O atom

in the aldehyde group [17]. The adsorbed C=O bond on the O_{vac} site is hydrogenated by the dissociative hydrogen on the neighboring Pt. As suggested by XPS measurements, Pt with oxychlorine precursors are coordinated by the O atom of the lanthanum support and remain unreduced as Pt^{2+} even after 600 °C reduction [45].

Upon Fe addition, some Pt–O bonds are broken depending on the H_2-treatment conditions and chemical surroundings of Pt cluster [36]. Concerning the H_2-TPR measurement, it can be seen that the promotional effect of iron on the increasing number of active hydrogen species due to the enhanced hydrogen spillover phenomenon [39]. The decrease in the Pt^{2+}/Pt^0 ratio provides further evidence of the promoted reducibility in the Fe-doped catalysts. As suggested by the XPS results, an increased electron density on metallic Pt is detected, which is reported to enhance the repulsive four-electron interactions with the C=C bond and favor a *d*-electron donation to the π* orbital of the polar C=O bond [49]. In addition, the positively charged $Fe^{\delta+}$ species as Lewis acid adsorption sites, would prefer the adsorption and activation of the C=O bond towards the improved production of unsaturated alcohol [42, 50]. Evidently, the hydrogenation rate of C=O bond on the $Pt^{\delta-}$–$Fe^{\delta+}$ couple outperforms the Pt–O_{vac} couple on the Pt/LOC, greatly improving the alcohol selectivity at low Fe loading of 0.25%. With the increment in Fe loading, more FeO_x or Pt–FeO_x particles with decreased size are constituted. As expected, the carbonyl hydrogenation is substantially improved accompanied by the evident decrease of BUAL and BUOL formation. Especially, the increase of carbonyl selectivity is predominant at Fe loadings of 0.25–0.50%. As a function of activity, at low Fe loading (0.25%), the prevailing effect of Fe is that of activating the substrate through a polarization of the carbonyl groups, which can react more easily with hydrogen chemisorbed on Pt. However, a further increase in Fe loading reduces the accessibility of Pt centers for hydrogen chemisorption because of the site blocking effect of Pt by metal oxide [51]. Accordingly, the total reactivity of CRAL hydrogenation is greatly decreased. Analogous composition-dependency of hydrogenation results has been reported on the selective hydrogenation of unsaturated aldehyde over active carbon-supported Pt–Sn catalysts and Rh–Sn/SiO_2 [43, 52]. Therefore, it seems that there is an optimum of surface Fe concentration allowing for the best catalytic reactivity and selectivity on the Fe-promoted Pt catalysts.

Conclusions

In the chemoselective hydrogenation of CRAL, incorporating Fe into the Pt/LOC catalyst is an effective way to improve the carbonyl reactivity. Upon hydrogen reduction, by varying Fe loading, the geometric and electronic characteristics of metals are modified owing to the composition-dependent interaction between Pt and FeO_x, which dominates the hydrogenation reactivity and selectivity. The suitable Pt–FeO_x interaction is likely to change the adsorption mode of CRAL molecules and contributes to the selective hydrogenation routes. This structure–activity study of PtFe/LOC catalysts provides new evidence and insight into the design and fabrication of bimetallic surfaces for specific reaction.

Acknowledgements The authors sincerely acknowledge the financial support from Innovation Promotion Association CAS (2017460), the National Science Foundation of China (21401204), the Science and Technology Project of Suzhou City (SYG201627) and the Western Light Program of Chinese Academy of Sciences (2015).

References

1. Gallezot P, Richard D (1998) Selective hydrogenation of α, β-unsaturated aldehydes. Catal Rev 40(1–2):81–126. doi:10.1080/01614949808007106
2. Claus P (1998) Selective hydrogenation of α, β-unsaturated aldehydes and other C=O and C=C bonds containing compounds. Top Catal 5(1):51–62. doi:10.1023/A:1019177330810
3. Ertl G, Knoezinger H, Schueth F, Weitkamp J (2008) Handbook of heterogeneous catalysis. Wiley, Germany
4. Vannice MA, Sen B (1989) Metal-support effects on the intramolecular selectivity of crotonaldehyde hydrogenation over platinum. J Catal 115(1):65–78. doi:10.1016/0021-9517(89)90007-9
5. Abid M, Paul-Boncour V, Touroude R (2006) Pt/CeO_2 catalysts in crotonaldehyde hydrogenation: selectivity, metal particle size and SMSI states. Appl Catal A 297(1):48–59. doi:10.1016/j.apcata.2005.08.048
6. Bhogeswararao S, Srinivas D (2012) Intramolecular selective hydrogenation of cinnamaldehyde over CeO_2–ZrO_2-supported Pt catalysts. J Catal 285(1):31–40. doi:10.1016/j.jcat.2011.09.006
7. Dandekar A, Vannice MA (1999) Crotonaldehyde hydrogenation on Pt/TiO_2 and Ni/TiO_2 SMSI catalysts. J Catal 183(2):344–354. doi:10.1006/jcat.1999.2419
8. Gebauerhenke E, Grams J, Szubiakiewicz E, Farbotko J, Touroude R, Rynkowski J (2007) Pt/Ga_2O_3 catalysts of selective hydrogenation of crotonaldehyde. J Catal 250(2):195–208. doi:10.1016/j.jcat.2007.06.021
9. Ruppert AM, Paryjczak T (2007) Pt/ZrO_2/TiO_2 catalysts for selective hydrogenation of crotonaldehyde: tuning the SMSI effect for optimum performance. Appl Catal A 320:80–90. doi:10.1016/j.apcata.2006.12.019
10. Sun Z, Rong Z, Wang Y, Xia Y, Du W, Wang Y (2014) Selective hydrogenation of cinnamaldehyde over Pt nanoparticles deposited on reduced graphene oxide. RSC Adv 4(4):1874–1878. doi:10.1039/c3ra44962a
11. Ammari F, Lamotte J, Touroude R (2004) An emergent catalytic material: Pt/ZnO catalyst for selective hydrogenation of crotonaldehyde. J Catal 221(1):32–42. doi:10.1016/S0021-9517(03)00290-2
12. Murillo LE, Chen JG (2008) A comparative study of the adsorption and hydrogenation of acrolein on Pt(111), Ni(111) film and Pt-Ni-Pt(111) bimetallic surfaces. Surf Sci 602(4):919–931. doi:10.1016/j.susc.2007.12.020
13. Merlo AB, Vetere V, Ruggera JF, Casella ML (2009) Bimetallic PtSn catalyst for the selective hydrogenation of furfural to furfuryl alcohol in liquid-phase. Catal Commun 10(13):1665–1669. doi:10.1016/j.catcom.2009.05.005
14. Shi J, Zhang M, Du W, Ning W, Hou Z (2015) SnO_2-isolated Pt_3Sn alloy on reduced graphene oxide: an efficient catalyst for selective hydrogenation of C=O in unsaturated aldehydes. Catal Sci Technol 5(6):3108–3112. doi:10.1039/c5cy00393h
15. Taniya K, Jinno H, Kishida M, Ichihashi Y, Nishiyama S (2012) Preparation of Sn-modified silica-coated Pt catalysts: a new PtSn bimetallic model catalyst for selective hydrogenation of crotonaldehyde. J Catal 288:84–91. doi:10.1016/j.jcat.2012.01.006
16. Englisch M, Jentys A, Lercher JA (1997) Structure sensitivity of the hydrogenation of crotonaldehyde over Pt/SiO_2 and Pt/TiO_2. J Catal 166(1):25–35. doi:10.1006/jcat.1997.1494
17. Kennedy G, Baker LR, Somorjai GA (2014) Selective amplification of C=O bond hydrogenation on Pt/TiO_2: catalytic reaction and sum-frequency generation vibrational spectroscopy studies of crotonaldehyde hydrogenation. Angew Chem Int Ed Engl 53(13):3405–3408. doi:10.1002/anie.201400081
18. Stassi JP, Zgolicz PD, de Miguel SR, Scelza OA (2013) Formation of different promoted metallic phases in PtFe and PtSn catalysts supported on carbonaceous materials used for selective hydrogenation. J Catal 306:11–29. doi:10.1016/j.jcat.2013.05.029

19. Coloma F, Llorca J, Homs N, de la Piscina PR, Rodriguez-Reinoso F, Sepulveda-Escribano A (2000) Crotonaldehyde hydrogenation over alumina- and silica-supported Pt–Sn catalysts of different composition. In situ DRIFT study. Phys Chem Chem Phys 2(13):3063–3069. doi:10.1039/B002005M
20. Mahata N, GonÃ§alves F, Pereira MFR, Figueiredo JLS (2008) Selective hydrogenation of cinnamaldehyde to cinnamyl alcohol over mesoporous carbon supported Fe and Zn promoted Pt catalyst. Appl Catal A 339(2):159–168. doi:10.1016/j.apcata.2008.01.023
21. Oduro WO, Cailuo N, Yu KMK, Yang H, Tsang SC (2011) Geometric and electronic effects on hydrogenation of cinnamaldehyde over unsupported Pt-based nanocrystals. Phys Chem Chem Phys 13(7):2590–2602. doi:10.1039/C0CP01832E
22. Bertero NM, Trasarti AF, Moraweck B, Borgna A, Marchi AJ (2009) Selective liquid-phase hydrogenation of citral over supported bimetallic Pt–Co catalysts. Appl Catal A 358(1):32–41. doi:10.1016/j.apcata.2009.01.036
23. Margitfalvi JL, Borbáth I, Hegedüs M, Tompos A (2002) Preparation of new type of Sn-Pt/SiO_2 catalysts for carbonyl activation. Appl Catal A 229(1–2):35–49. doi:10.1016/S0926-860X(02)00014-5
24. Merlen E, Beccat P, Bertolini JC, Delichäre P, Zanier N, Didillon B (1996) Characterization of bimetallic Pt-Sn/Al_2O_3 catalysts: relationship between particle size and structure. J Catal 159(1):178–188. doi:10.1006/jcat.1996.0077
25. Rong H, Niu Z, Zhao Y, Cheng H, Li Z, Ma L, Li J, Wei S, Li Y (2015) Structure evolution and associated catalytic properties of Pt–Sn bimetallic nanoparticles. Chem Eur J 21(34):12034–12041. doi:10.1002/chem.201501442
26. Hou Y-H, Han W-C, Xia W-S, Wan H-L (2015) Structure sensitivity of $La_2O_2CO_3$ catalysts in the oxidative coupling of methane. ACS Catal 5(3):1663–1674. doi:10.1021/cs501733r
27. Levan T, Che M, Tatibouet JM, Kermarec M (1993) Infrared study of the formation and stability of $La_2O_2CO_3$ during the oxidative coupling of methane on La_2O_3. J Catal 142(1):18–26. doi:10.1006/jcat.1993.1185
28. Huang X, Dang C, Yu H, Wang H, Peng F (2015) Morphology effect of Ir/$La_2O_2CO_3$ nanorods with selectively exposed 110 facets in catalytic steam reforming of glycerol. ACS Catal 5(2):1155–1163. doi:10.1021/cs5014305
29. Du X, Zhang D, Shi L, Gao R, Zhang J (2012) Morphology dependence of catalytic properties of Ni/CeO_2 nanostructures for carbon dioxide reforming of methane. J Phys Chem 116(18):10009–10016. doi:10.1021/jp300543r
30. Hou F, Zhao H, Zhao J, Yang J, Yan L, Song H, Chou L (2016) Morphological effect of lanthanum-based supports on the catalytic performance of Pt catalysts in crotonaldehyde hydrogenation. J Nanopart Res 18(3):1–17. doi:10.1007/s11051-016-3373-6
31. Irusta S, Cornaglia LM, Lombardo EA (2004) Effects of rhodium and platinum on the reactivity of lanthanum phases. Mater Chem Phys 86(2–3):440–447. doi:10.1016/j.matchemphys.2004.04.017
32. Irusta S, Cornaglia LM, Lombardo EA (2002) Hydrogen production using Ni–Rh on La_2O_3 as potential low-temperature catalysts for membrane reactors. J Catal 210(1):7–16. doi:10.1006/jcat.2002.3612
33. Faroldi BM, Mánera JF, Cornaglia LM (2014) In situ characterization of phase transformation and reactivity of high surface area lanthanum-based Ru catalysts for the combined reforming of methane. Appl Catal B 150–151:126–137. doi:10.1016/j.apcatb.2013.12.005
34. Silvestre-Albero J, Coloma F, Sepúlveda-Escribano A, Rodríguez-Reinoso F (2006) Effect of the presence of chlorine in bimetallic PtZn/CeO_2 catalysts for the vapor-phase hydrogenation of crotonaldehyde. Appl Catal A 304:159–167. doi:10.1016/j.apcata.2006.02.039
35. Zhou Y, Doronkin DE, Chen M, Wei S, Grunwaldt J-D (2016) Interplay of Pt and crystal facets of TiO_2: CO oxidation activity and operando XAS/DRIFTS studies. ACS Catal 6(11):7799–7809. doi:10.1021/acscatal.6b01509
36. Yakovina OA, Lisitsyn AS (2016) Probing the H_2-induced restructuring of Pt nanoclusters by H_2-TPD. Langmuir 32(46):12013–12021. doi:10.1021/acs.langmuir.6b02847
37. Guczi L (2005) Bimetallic nano-particles: featuring structure and reactivity. Catal Today 101(2):53–64. doi:10.1016/j.cattod.2005.01.002
38. Gao Y, Wang W, Chang S, Huang W (2013) Morphology effect of CeO_2 support in the preparation, metal-support interaction, and catalytic performance of Pt/CeO_2 catalysts. ChemCatChem 5(12):3610–3620. doi:10.1002/cctc.201300709
39. Hossain MM (2006) Influence of noble metals (Rh, Pd, Pt) on Co-saponite catalysts for HDS and HC of heavy oil. Chem Eng J 123(1–2):15–23. doi:10.1016/j.cej.2006.07.003

40. Chen P, Lu J, Xie G, Zhu L, Luo M (2012) Characterizations of Ir/TiO_2 catalysts with different Ir contents for selective hydrogenation of crotonaldehyde. Reac Kinet Mech Cat 106(2):419–434. doi:10.1007/s11144-012-0435-3
41. Fernandes DM, Scofield CF, Alcover Neto A, Cardoso MJB, Zotin JL, Zotin FMZ (2012) The hydrogen adsorption capacity of commercial Pd/Rh and Pt/Rh automotive catalysts and its relationship to their activity. Chem Eng J 189–190:62–67. doi:10.1016/j.cej.2012.02.024
42. Shi Y-S, Yuan Z-F, Wei Q, Sun K-Q, Xu B-Q (2016) Pt–FeO_x/SiO_2 catalysts prepared by galvanic displacement show high selectivity for cinnamyl alcohol production in the chemoselective hydrogenation of cinnamaldehyde. Catal Sci Technol 6(19):7033–7037. doi:10.1039/C6CY01340F
43. Neri G, Donato A, Milone C, Mercadante L, Visco AM (1994) Selective hydrogenation of citral over Pt–Sn supported on activated carbon. J Chem Technol Biotechnol 60(1):83–88. doi:10.1002/jctb.280600113
44. Bäumer M, Freund H-J (1999) Metal deposits on well-ordered oxide films. Prog Surf Sci 61(7–8):127–198. doi:10.1016/S0079-6816(99)00012-X
45. Lee J, Ryou Y, Chan X, Kim TJ, Kim DH (2016) How Pt interacts with CeO_2 under the reducing and oxidizing environments at elevated temperature: the origin of improved thermal stability of Pt/CeO_2 compared to CeO_2. J Phys Chem C 120(45):25870–25879. doi:10.1021/acs.jpcc.6b08656
46. Salgado JRC, Duarte RG, Ilharco LM, Botelho do Rego AM, Ferraria AM, Ferreira MGS (2011) Effect of functionalized carbon as Pt electrocatalyst support on the methanol oxidation reaction. Appl Catal B 102(3–4):496–504. doi:10.1016/j.apcatb.2010.12.031
47. Qiao B, Wang A, Yang X, Allard LF, Jiang Z, Cui Y, Liu J, Li J, Zhang T (2011) Single-atom catalysis of CO oxidation using Pt_1/FeO_x. Nat Chem 3(8):634–641. doi:10.1038/nchem.1095
48. Li X, Li D, Tian H, Zeng L, Zhao Z-J, Gong J (2017) Dry reforming of methane over Ni/La_2O_3 nanorod catalysts with stabilized Ni nanoparticles. Appl Catal B 202:683–694. doi:10.1016/j.apcatb.2016.09.071
49. Hsu C-Y, Chiu T-C, Shih M-H, Tsai W-J, Chen W-Y, Lin C-H (2010) Effect of electron density of Pt catalysts supported on alkali titanate nanotubes in cinnamaldehyde hydrogenation. J Phys Chem C 114(10):4502–4510. doi:10.1021/jp9095198
50. Yuan J-F, Luo C-Q, Yu Q, Jia A-P, Hu G-S, Lu J-Q, Luo M-F (2016) Great improvement on the selective hydrogenation of crotonaldehyde over CrO_x- and FeO_x-promoted Ir/SiO_2 catalysts. Catal Sci Technol 6(12):4294–4305. doi:10.1039/C6CY00012F
51. Chen N, Ren Y, Qian EW (2016) Elucidation of the active phase in PtSn/SAPO-11 for hydrodeoxygenation of methyl palmitate. J Catal 334:79–88. doi:10.1016/j.jcat.2015.11.001
52. Reyes P, Aguirre MC, Fierro JLG, Santori G, Ferretti O (2002) Hydrogenation of crotonaldehyde on Rh–Sn/SiO_2 catalysts prepared by reaction of tetrabutyltin on prereduced Rh/SiO_2 precursors. J Mol Catal A 184(1–2):431–441. doi:10.1016/S1381-1169(02)00031-6